

Towards the engineering of a Quantum Key Distribution receiver robust to ambient light

Vincent Lee*, Andy Schreier, Grahame Faulkner, Dominic O'Brien

Optical Wireless Communications group, Department of Engineering Science, University of Oxford
OX1 3PJ, UK

ABSTRACT

Quantum Key Distribution (QKD) has the potential to secure indoor optical wireless links. In a typical room scenario, an indoor optical wireless link will have a transmitter on the ceiling and a receiver on a desk. Ambient light from room (typically LED) lighting on the ceiling and sunlight coming through the windows present a challenging environment for free-space QKD links to operate, and a key challenge is to mitigate the noise induced by ambient light, particularly sunlight. A combination of spectral and spatial filtering can be used to reduce the effect of ambient light, with a narrowband optical filter typically used. Moreover, the wavelength of operation is key to further reduce the impact of ambient light. Wavelengths in 'quiet' regions of the solar spectrum, such as the atmospheric absorption bands, are promising candidates. We are currently working on a system that operates at 1370 nm, where water and carbon dioxide absorption band in the atmosphere attenuate the solar spectrum substantially. This paper reports the design and modelling of the system, with a series of validation measurements to characterise the effect of solar radiation on a typical photon-counting detector as would be used in a QKD system. The aim of this work is to show the feasibility of the wavelength region around 1370 nm as a necessary step towards a low noise QKD receiver for indoor optical wireless links in a practical environment.

Keywords: QKD, indoor optical wireless, 1370 nm, robust to ambient light

1. INTRODUCTION

Quantum Key Distribution (QKD) has the potential to secure indoor optical wireless links. QKD uses the properties of quantum mechanics, such as the no cloning theorem [1], and the ability to detect an eavesdropper to guarantee security [2]. QKD has been used in long distance fibre [3], free-space [4], and short range handheld experiments [5-9]. A major difference between fibre and free-space quantum communications is ambient light, mainly sunlight and its effect on a QKD receiver by inducing additional photon counts which must be treated as noise. Free-space QKD experiments have been conducted outdoors in the presence of sunlight [10-14] and these experiments show that sunlight can impair the performance of a QKD link.

In a typical room scenario, an indoor optical wireless link will have a transmitter on the ceiling and a receiver on a desk. LED lighting on the ceiling and sunlight coming through the windows are typical sources of ambient light for such links. Indoor QKD links under LED lighting have been investigated previously [15, 16], and a key challenge is to mitigate the noise induced by ambient light, in particular sunlight, at the QKD receiver to operate a QKD link. The reduction of this noise can be achieved by spectral and spatial filtering, with a narrowband optical filter typically used. Moreover, the wavelength of operation is key to further reduce the impact of ambient light. Wavelengths in a 'quiet' region of the solar spectrum such as the atmospheric absorption bands [17] are promising candidates. More precisely, the water and carbon dioxide absorption band (1351 – 1414 nm) is of interest. In this work, we consider the design and modelling of the system, with a series of validation measurements to characterise the effect of solar radiation on a typical photon-counting detector as would be used in a QKD system. We investigated the wavelength region of 1351 – 1414 nm on a sunny day by measuring the photon counts per second in direct sunlight using a 10 nm interference filter centred at 1370 nm, single mode fibre with collimator, and an IDQ idQube SPAD [18]. A similar experiment was undertaken under LED ceiling lighting in a lab.

*vincent.lee@eng.ox.ac.uk; phone +44(0) 7397-138883;

2. EXPERIMENTAL METHOD

2.1 Spectral region of interest

Figure 1 shows the ASTM Air Mass 1.5 spectrum [19] in $\text{photons.s}^{-1}.\text{m}^{-2}$ vs wavelength. The ASTM AM1.5 standard is a spectrum of the average solar irradiance (W/m^2) in 2π steradian field of view for sunlight travelling through an atmospheric density of 1.5 times the atmosphere at sea level [20]. The solar irradiance is converted to $\text{photons.s}^{-1}.\text{m}^{-2}$ based on the photon energy at each wavelength. The Earth's atmosphere attenuates the sunlight according to its wavelengths, creating absorption bands. The area highlighted in the box is the water and carbon dioxide absorption band and is the primary region of interest in this paper due to the minimal photon counts between 1351 – 1414 nm. It can be seen in Figure 1b that a narrowband region around 1370 nm has the lowest number of photon counts in this band.

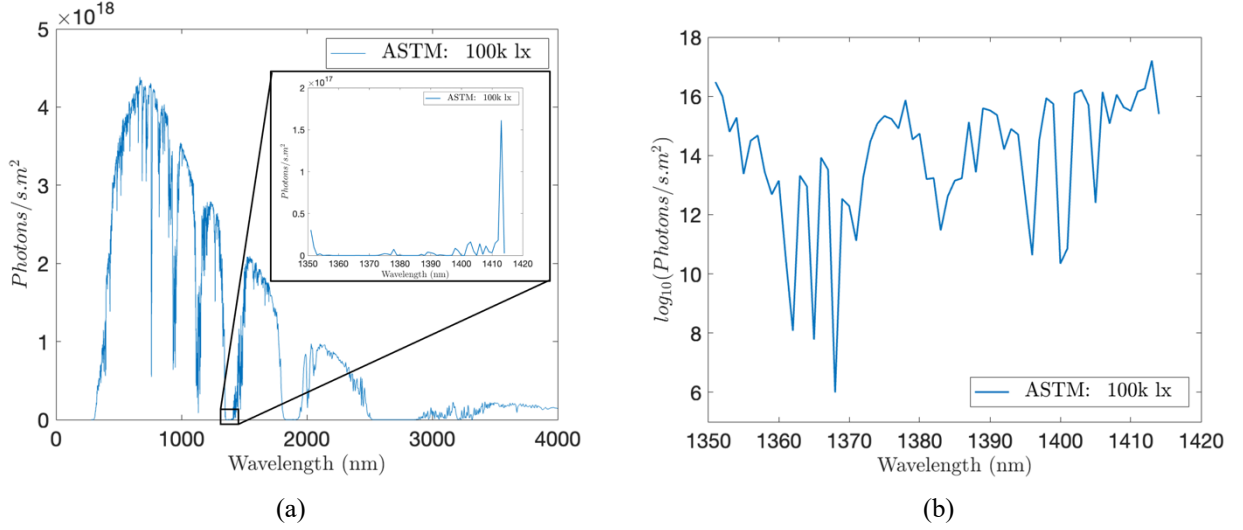


Figure 1. (a) Plot of ASTM AM1.5 spectrum at 100k lx in $\text{photons.s}^{-1}.\text{m}^{-2}$ vs wavelength and (b) 1351 – 1414 nm region in $\log_{10}(\text{photons.s}^{-1}.\text{m}^{-2})$ vs wavelength.

In a previous publication, we reported results from a simulated indoor QKD link for a typical office environment with a transmitter on the ceiling and a receiver on the floor [21]. The simulation assumed indoor ambient light levels of LED lighting at 500 lx and sunlight at 1,000 lx. Effectively, there is no effect from LEDs in the water and carbon dioxide absorption band due to the emission wavelengths of the LED ranging from 400 – 800 nm. The simulation results showed that a QKD link with a transmitted spot $\leq \varnothing 3$ mm and a receiver with 9.3 nm filter bandwidth could operate at a Quantum Bit Error Rate (QBER) of 4%. The maximum QBER threshold for BB84 is 11% [22, 23].

2.2 Experimental setup

The rest of this paper will focus on a set of experiments to measure the photon counts per second (CPS) induced by outdoor and indoor ambient light and the potential effect on a QKD receiver. Figure 2 shows the experimental apparatus in three scenarios: a) on a terrace outside a meeting room under clear skies (100k lx), b) under cloudy skies (30k lx), and c) inside the meeting room (12k lx). The experimental apparatus consisted of a calibrated NIR Flame spectrometer with $\varnothing 600$ μm fibre and cosine corrector used to measure the spectrum, an IDQ idQube SPAD with a single mode fibre input used to count photons, and an Amprobe LM-100 lux meter used to measure the lux levels. The spectrometer and the SPAD fibre inputs were fixed on a post that directed them towards the same source. At the front end of the single mode fibre is a 10 nm passband filter centred at 1370 nm (Spectrogon NB-1370-010 [24]) and collimator with $\varnothing 6$ mm aperture (Thorlabs F280FC-C). The SPAD operated in free-running mode at 25 μs deadtime and 10% detection efficiency with dark counts of 500 CPS on average. For comparison, a similar experiment was conducted to measure the LED ceiling lighting in a lab. The experimental apparatus was placed directly on the ceiling light which the lux meter recorded at 100k lx close to the LED sources.

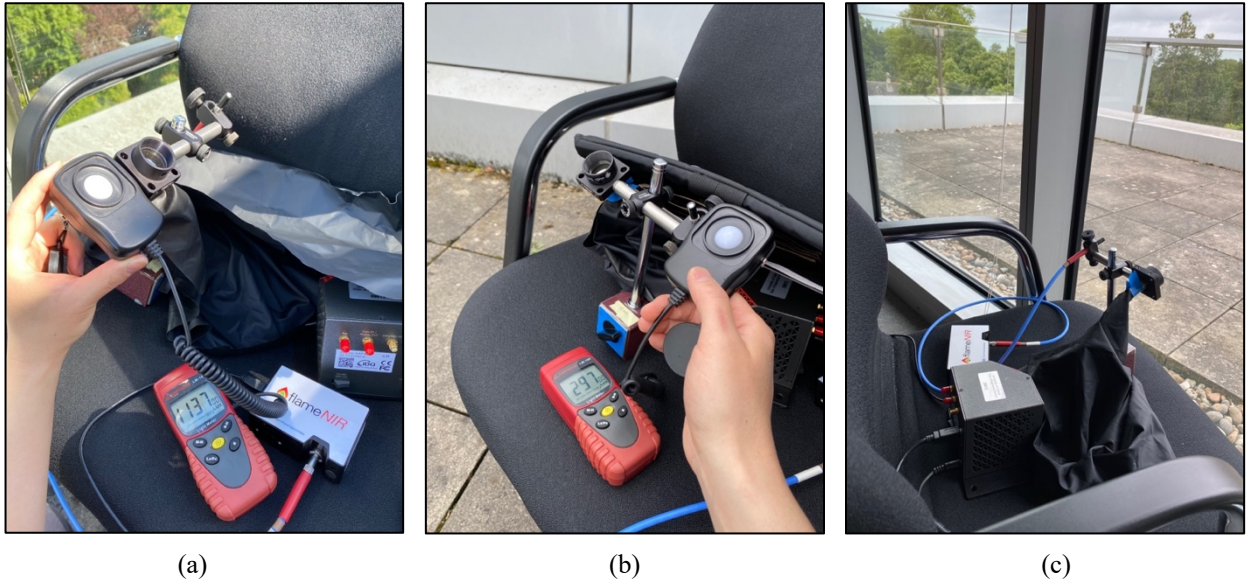


Figure 2. The experimental apparatus used to measure photon counts per second, the spectrum, and lux levels in three scenarios: (a) outside under clear skies at 100k lx in direct sunlight, (b) outside under cloudy skies at 30k lx, (c) inside a meeting room at 12k lx.

Figure 3 shows the measured spectra captured by the NIR Flame spectrometer in $\text{photons.s}^{-1}.\text{m}^{-2}$ vs wavelength and the ASTM AM1.5 spectrum for reference. The measured spectra shown are from the three scenarios in Figure 2 and the spectrum measured under LED ceiling lighting in a lab. The spectrometer is calibrated for irradiance (W/m^2) over a bandwidth of 1015 – 1654 nm with a cosine corrector that has 2π steradian field of view. The spectra are converted from irradiance to $\text{photons.s}^{-1}.\text{m}^{-2}$.

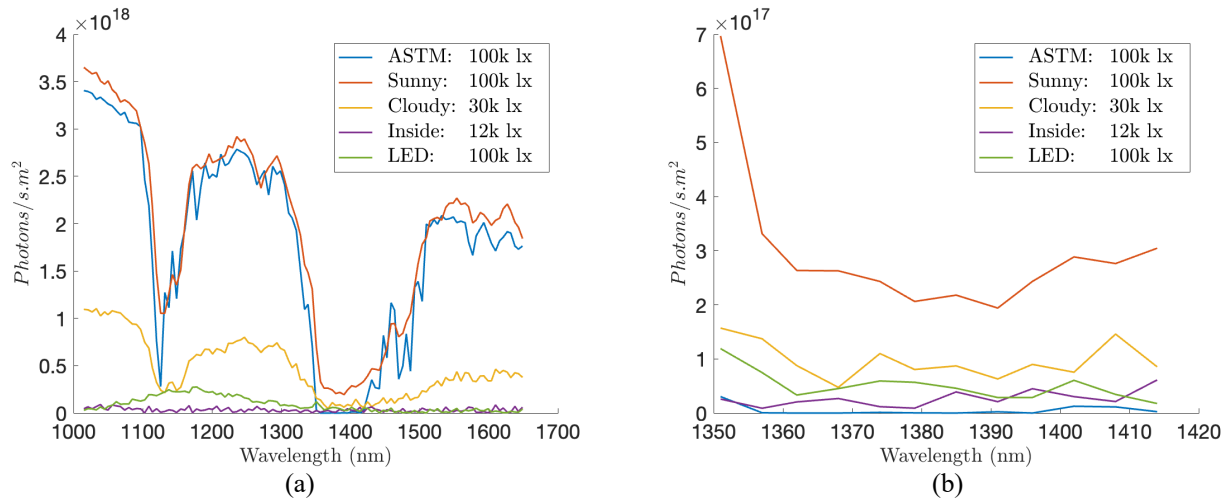


Figure 3. (a) Plot of measured spectra by the NIR Flame spectrometer and the ASTM AM1.5 spectrum (as reference) in $\text{photons.s}^{-1}.\text{m}^{-2}$ vs wavelength and (b) 1351 – 1414 nm region in $\text{photons.s}^{-1}.\text{m}^{-2}$ vs wavelength. The plots show the measured spectra for the three scenarios in Figure 2 and the measured spectrum under LED ceiling lighting in a lab.

3. RESULTS AND DISCUSSION

3.1 Spectrum and SPAD measurements

Table 1 shows the estimated and measured photon counts per second. The top three rows of Table 1 show the estimated total photon counts the SPAD would receive using the NIR Flame spectrometer measurements. The estimates are for three wavelength ranges: 1) the bandwidth of the spectrometer (1015 – 1654 nm), 2) the region of interest (1351 – 1414 nm), and 3) the 10 nm passband of the Spectrogon filter (1367 – 1377 nm). It is assumed the SPAD has 10% photon detection efficiency across all wavelengths. The photon counts were estimated by multiplying the unfiltered measured spectra in Figure 3 with the 10% photon detection efficiency across all wavelengths. Next, the spectra were multiplied by $1/2\pi$ steradians to remove the cosine corrector field of view. Then the spectra were multiplied by the etendue of the SPAD which consisted of a $\varnothing 9 \mu\text{m}$ single mode fibre with numerical aperture of 0.1. Finally, the resultant spectra in photon counts. s^{-1} vs wavelength were multiplied with the transmittance values found in the Spectrogon 10 nm passband filter datasheet for wavelengths 1015 – 1654 nm and integrated across the three wavelength ranges to estimate the total photon counts per second.

The bottom two rows of Table 1 show the measured photon counts per second from the idQube SPAD. The maximum measurements were obtained by directing the experimental apparatus towards the source to ensure the maximum number of photons were entering into the SPAD. The minimum measurements were obtained by directing the apparatus away from the source, e.g. in the case of direct sunlight, the apparatus was pointed away from the sun and up towards the clear sky. The measurement readings were stable and averaged over two minutes.

Table 1. Estimated and measured photon counts per second

Type of measurement	Range of measurement	Outside Sunny 100k lx	Outside Cloudy 30k lx	Inside 12k lx	LED lighting 100k lx
Spectrum	1015 – 1654 nm	6,426	1,994	389	1,160
Spectrum	1351 – 1414 nm	5,242	1,759	373	1,115
Spectrum	1367 – 1377 nm	3,828	1,437	241	861
SPAD	Maximum	7,000	1,800	500	900
SPAD	Minimum	2,000	1,300	500	500

There is variation between the measured and estimated data for ambient light at 100k lx, 30k lx, and 12k lx. It can be seen that

1) The ‘Sunny: 100k lx’ spectrum tracks well with the ASTM standard and the ‘Cloudy: 30k lx’ spectrum is as expected in terms of scale. The estimated photon counts for these spectra from 1015 – 1654 nm are in good agreement with the maximum measured photon counts. The estimated counts for the ‘Sunny: 100k lx’ spectrum is 6,426 CPS which is comparable to the measured maximum 7,000 CPS. Similarly, the estimated counts for the ‘Cloudy: 30k lx’ spectrum is 1,994 CPS which is comparable to the measured maximum 1,800 CPS.

2) There are a significant number of photon counts due to filter leakage outside of the passband of the filter (1367 – 1377 nm). Although the Spectrogon filter has OD3 sideband suppression outside of the 10 nm passband, it is possible to stack a short pass and long pass filter on top of the passband filter to further reduce the leakage.

3) The ‘Inside: 12k lx’ spectrum, measured inside the meeting room, is different from the outdoor solar spectra due to the coating on the double-glazed windows. The estimated photon counts for the ‘Inside: 12k lx’ spectrum are below the 500 dark counts of the SPAD. The SPAD measurements show there is no ambient light induced noise at the SPAD. Hence, the dark counts are the dominant noise factor.

4) The estimated photon counts based on the ‘LED: 100k lx’ spectrum, measured directly on the ceiling lighting inside a lab, is in good agreement with the SPAD measurements. The estimated counts for the ‘LED: 100k lx’ spectrum is 1,160 CPS which is comparable to the measured maximum 900 CPS.

3.2 Impact on a QKD receiver

Figure 4 shows the receiver design based on the BB84 protocol which was first introduced by C. H. Bennett and G. Brassard in 1984 [25]. It is a discrete variable QKD protocol where Alice sends qubits based on polarisation (Horizontal, Vertical, Diagonal, Anti-diagonal) to Bob over a quantum channel. Each qubit is one of a pair of orthogonal bases. Bob measures each qubit sent by Alice with a pair of orthogonal bases, Horizontal/Vertical or Diagonal/Anti-diagonal. At the entrance of the receiver, a spectral filter (Spectrogon 10 nm passband filter) centred at 1370 nm is used to mitigate the ambient light entering the receiver. A non-polarising beam splitter is used to facilitate Bob’s choice of basis pair. One branch of the receiver consists of a polarising beam splitter to choose between Horizontal and Vertical basis. The other branch consists of a half wave plate and polarising beam splitter to choose between Diagonal and Anti-diagonal basis. Right Angle Mirrors are used to ensure high efficiency coupling at the collimators with the single mode fibres and SPADs.

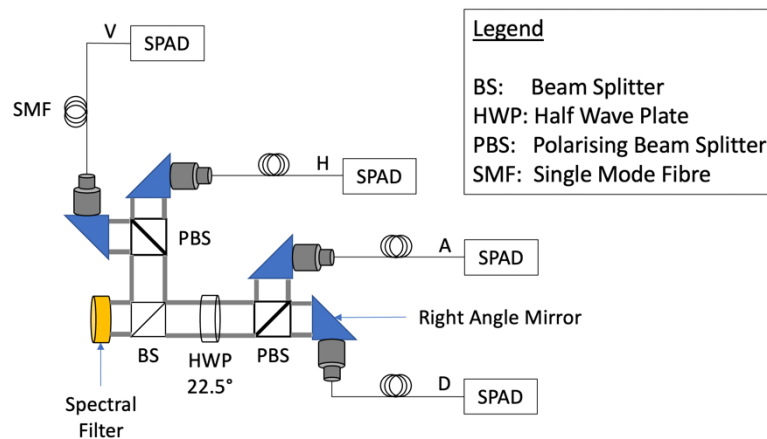


Figure 4: BB84 receiver design

As shown in Table 1, there are minimal photon counts per second in the region around 1370 nm, both outdoors and indoors. In the worst-case scenario with direct sunlight, the number of photons that would enter each SPAD can be extrapolated considering the receiver design in Figure 4. The photon counts get halved after the 50:50 beam splitter and then halved again after the polarising beam splitter prior to entering each collimator. The photon counts can be reduced from a maximum of 7,000 to 1,750 CPS per SPAD. For cloudy skies, the maximum drops from 1,800 to 450 CPS which is below the 500 dark counts of the SPAD. This is similar for the indoor measurements. For sunlight through double-glazed windows, the maximum drops from 500 to 125 CPS and for LED lighting at 100k lx, the maximum drops from 900 to 225 CPS. All of the measurements are dominated by the dark counts of the SPAD, except for the outdoor maximum in direct sunlight at 100k lx. Therefore, ambient light has minimal effect on the QKD receiver around 1370 nm.

Based on the presented receiver design and measured photon counts per second in Table 1, the QBER of a QKD link can be estimated. The equations (1) – (4) can be used to estimate the QBER and can be found in Section IV A in [2]. R_{sift} is the sifted raw key rate, R_{opt} is the intrinsic error rate of the QKD setup due to the probability of the sifted photon entering the wrong detector, and R_{det} is the total noise count rate across all of the detectors. The parameters are factor $q = 1$ for non-phase coding setup, repetition rate $f_{rep} = 100e6$, mean photon number $\mu = 0.1$, detector efficiency $\eta = 0.1$, polarisation contrast $p_{opt} = 0.01$, and number of detectors $n = 4$. t_{link} is defined as the link loss. p_{noise} is the probability of the total noise counts per time window per SPAD that include the dark counts and the sunlight.

$$R_{sift} = \frac{1}{2} q f_{rep} \mu t_{link} \eta \quad (1)$$

$$R_{opt} = R_{sift} p_{opt} \quad (2)$$

$$R_{det} = \frac{1}{2} f_{rep} p_{noise} n \quad (3)$$

$$QBER = \frac{R_{opt} + R_{det}}{R_{sift}} = p_{opt} + \frac{p_{noise} \cdot n}{t_{link} \cdot \eta \cdot 2 \cdot q \cdot \mu} \quad (4)$$

Figure 5 shows a plot of the estimated QBER based on the total noise counts at the SPAD and the effect of varying link losses t_{link} . It can be seen in Figure 5 that a BB84 link with a 10 nm passband filter centred at 1370 nm could tolerate direct sunlight and operate well below the 11% threshold depending on the link loss. A practical QBER threshold to satisfy is 4% for a mean photon number $\mu = 0.1$ [2]. This threshold ensures that Alice and Bob have enough QBER margin to perform classical error correction and privacy amplification to guarantee security against Eve's individual attacks. Figure 5 shows that a QKD link can potentially operate in direct sunlight with QBER at 3% and potentially tolerate a 7 dB link loss. For higher light levels (and noise counts) lower link losses can be tolerated.

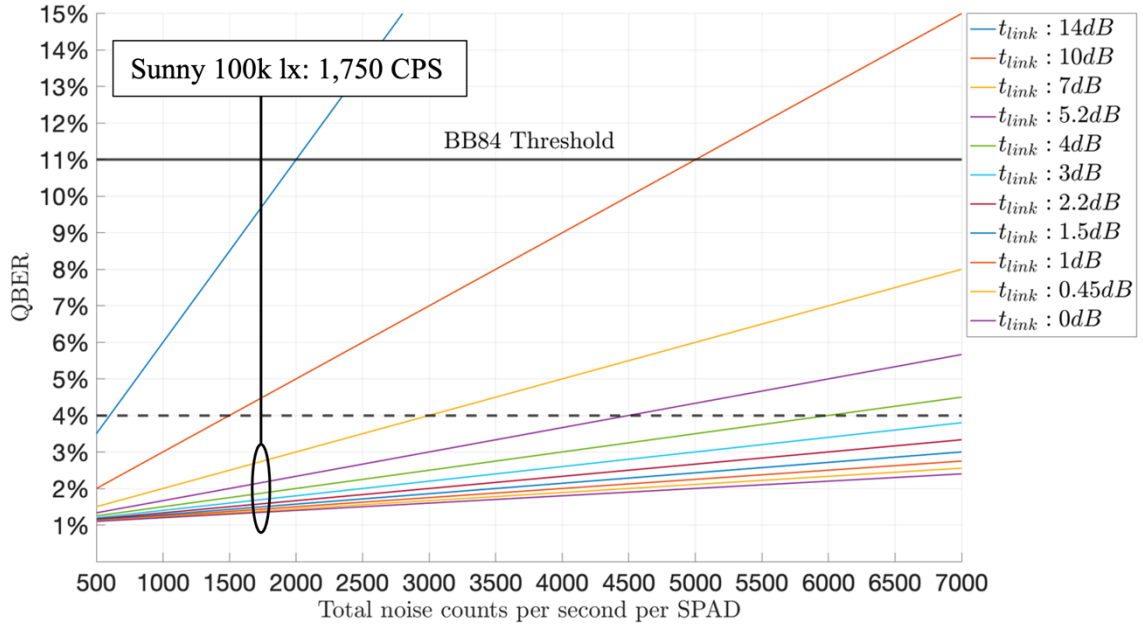


Figure 5. Plot of QBER vs total noise counts per second per SPAD. The QBER is estimated at various QKD link losses (t_{link}) in dB.

4. CONCLUSIONS AND FUTURE WORK

In this work, a wavelength region is proposed to operate a QKD link that is robust to ambient light and the influence of ambient light on the QKD link performance is investigated. The experimental measurements show that a BB84 link should operate at 1370 nm because the ambient light in this region has minimal effect on a QKD receiver based on the design in Figure 4. An additional advantage of 1370 nm is the proximity to telecommunications wavelengths as it can be used in standard single mode fibres [26] and the wavelength can be separated in conventional Coarse Wavelength Division Multiplexing (CWDM) systems through filtering [27]. Work is underway on an experiment that tests a QKD system, designed for 1370 nm and the BB84 protocol, with the receiver under a halogen lamp as an equivalent substitute for ambient sunlight in the 1351 – 1414 nm region.

REFERENCES

- [1] W. K. Wootters and W. H. Zurek, "A single quantum cannot be cloned," *Nature*, vol. 299, no. 5886, pp. 802-803, 1982/10/01 1982, doi: 10.1038/299802a0.
- [2] N. Gisin, G. Ribordy, W. Tittel, and H. Zbinden, "Quantum cryptography," *Reviews of modern physics*, vol. 74, no. 1, p. 145, 2002.
- [3] J.-P. Chen *et al.*, "Sending-or-Not-Sending with Independent Lasers: Secure Twin-Field Quantum Key Distribution over 509 km," *Physical Review Letters*, vol. 124, no. 7, p. 070501, 02/20/ 2020, doi: 10.1103/PhysRevLett.124.070501.
- [4] S.-K. Liao *et al.*, "Satellite-to-ground quantum key distribution," *Nature*, vol. 549, no. 7670, p. 43, 2017.
- [5] J. Duligall, M. Godfrey, K. Harrison, W. Munro, and J. Rarity, "Low cost and compact quantum key distribution," *New Journal of Physics*, vol. 8, no. 10, p. 249, 2006.
- [6] J. Wabnig, D. Bitauld, H. Li, A. Laing, J. O'Brien, and A. Niskanen, "Demonstration of free-space reference frame independent quantum key distribution," *New Journal of Physics*, vol. 15, no. 7, p. 073001, 2013.
- [7] H. Chun *et al.*, "Handheld free space quantum key distribution with dynamic motion compensation," *optics express*, vol. 25, no. 6, pp. 6784-6795, 2017.
- [8] D. Lowndes, S. Frick, A. Hart, and J. Rarity, "A low cost, short range quantum key distribution system," *EPJ Quantum Technology*, vol. 8, no. 1, p. 15, 2021/05/26 2021, doi: 10.1140/epjqt/s40507-021-00101-2.
- [9] D. Lowndes, A. Schreier, D. O'Brien, and J. Rarity, *Characterising a handheld quantum key distribution system with emulated beam steering* (SPIE Photonex). SPIE, 2021.
- [10] B. Jacobs and J. Franson, "Quantum cryptography in free space," *Optics Letters*, vol. 21, no. 22, pp. 1854-1856, 1996.
- [11] R. J. Hughes *et al.*, "Practical Free-Space Quantum Cryptography," 1999. University of California, Los Alamos National Laboratory.
- [12] R. J. Hughes, J. E. Nordholt, D. Derkacs, and C. G. Peterson, "Practical free-space quantum key distribution over 10 km in daylight and at night," *New journal of physics*, vol. 4, no. 1, p. 43, 2002.
- [13] S. Nauerth *et al.*, "Air-to-ground quantum communication," *Nature Photonics*, vol. 7, pp. 382-386, 2013.
- [14] C. Quintana *et al.*, *Low size, weight and power quantum key distribution system for small form unmanned aerial vehicles* (SPIE LASE). SPIE, 2019.
- [15] O. Elmabrok and M. Razavi, "Wireless quantum key distribution in indoor environments," *JOSA B*, vol. 35, no. 2, pp. 197-207, 2018.
- [16] O. Elmabrok, M. Ghalaii, and M. Razavi, "Quantum-classical access networks with embedded optical wireless links," *JOSA B*, vol. 35, no. 3, pp. 487-499, 2018.

- [17] I. N. Sokolik, "Absorption by atmospheric gases in the IR, visible and UV spectral regions," *School of Earth and Atmospheric Sciences, Georgia Institute of Technology [Online]*. Available: http://irina.eas.gatech.edu/EAS8803_Fall2009/Lec6.pdf, 2009.
- [18] id Quantique, "ID Qube NIR Free-Running SPAD."
- [19] ASTM G173-03(2020), *Standard Tables for Reference Solar Spectral Irradiances: Direct Normal and Hemispherical on 37° Tilted Surface*. West Conshohocken, PA: ASTM International, 2020.
- [20] C. Riordan and R. Hulstron, "What is an air mass 1.5 spectrum? (solar cell performance calculations)," in *IEEE Conference on Photovoltaic Specialists*, 21-25 May 1990 1990, pp. 1085-1088 vol.2.
- [21] V. Lee and D. O'Brien, "Indoor Optical Wireless Communications using Quantum Key Distribution at 1370 nm," in *2020 IEEE Photonics Conference (IPC)*, 28 Sept.-1 Oct. 2020 2020, pp. 1-2, doi: 10.1109/IPC47351.2020.9252396.
- [22] P. W. Shor and J. Preskill, "Simple Proof of Security of the BB84 Quantum Key Distribution Protocol," *Physical Review Letters*, vol. 85, no. 2, pp. 441-444, 07/10/ 2000, doi: 10.1103/PhysRevLett.85.441.
- [23] D. Mayers, "Shor and Preskill's and Mayers's security proof for the BB84 quantum key distribution protocol," *The European Physical Journal D - Atomic, Molecular, Optical and Plasma Physics*, vol. 18, no. 2, pp. 161-170, 2002/02/01 2002, doi: 10.1140/epjd/e20020020.
- [24] Spectrogon, "Narrow Bandpass Filters," 22 March 2018. [Online]. Available: <https://www.spectrogon.com/wp-content/uploads/spectrogon/NB-1370-010-nm.pdf>
- [25] C. H. Bennett and G. Brassard, "Quantum Cryptography: Public Key Distribution and Coin Tossing," presented at the International Conference on Computers, Systems & Signal Processing, Bangalore, India, December 9-12, 1984.
- [26] Corning. *Corning SMF-28 Ultra Optical Fiber*. (2021). [Online]. Accessed: 17 July 2022. [Online]. Available: <https://www.corning.com/media/worldwide/coc/documents/Fiber/product-information-sheets/PI-1424-AEN.pdf>
- [27] I. Choi, R. J. Young, and P. D. Townsend, "Quantum key distribution on a 10Gb/s WDM-PON," *Optics Express*, vol. 18, no. 9, pp. 9600-9612, 2010/04/26 2010, doi: 10.1364/OE.18.009600.